Kajol Maheshwari, *Sanjeev Sharma*

ELASTIC-PLASTIC TRANSITION IN FUNCTIONALLY GRADED THIN ROTATING ORTHOTROPIC DISK WITH EXPONENTIALLY VARIABLE THICKNESS AND VARIABLE DENSITY

ELASTOPLASTIČNI PRELAZNI NAPONI U TANKOM ROTIRAJUĆEM ORTOTROPNOM DISKU OD FUNKCIONALNOG MATERIJALA SA EKSPONENCIJALNIM PROMENAMA DEBLJINE I GUSTINE

Originalni naučni rad / Original scientific paper
UDK /UDC:

Rad primljen / Paper received: 12.12.2020

Adresa autora / Author's address:
Department of Mathematics, Jaypee Institute of Information Technology, Noida, India email:
kajolm.maths@gmail.com or sanjeev.sharma@jiit.ac.in

Keywords
- elastic, plastic
- exponentially variable
- thickness, density
- functionally graded rotating disk
- orthotropic material

Ključne reči
- elastičan, plastičan
- eksponencijalna promenljiva
- debljina, gustina
- rotirajući disk od funkcionalnog materijala
- ortotropni materijal

Abstract

A thin rotating functionally graded disk whose thickness and density varies exponentially has been investigated. Angular speed, radial stresses and circumferential stresses at initial yielding and fully plastic state have been obtained using transition theory which helps to eliminate the assumption of yield condition. On the basis of numerical and graphical analysis of angular speed and circumferential stresses, it has been found that for designing purposes, functionally graded disk made up of isotropic material (steel) with non-homogeneity parameter is a better option than functionally graded orthotropic disk (topaz and barite) as the disk of isotropic material with non-homogeneity parameter has less circumferential stress than that of orthotropic material.

Izvod

Istražen je tanki rotirajući disk od funkcionalnog materijala sa eksponencijalno promenljivom debljinom i gustinom. Teorijom prelaznih napona, čime je olakšano zanemarivanje stanja tečenja, dobijeni su: ugaona brzina, radijalni i obimski naponi pri tečenju i u stanju potpune plastičnosti. Na osnovu numeričke analize i grafičkog predstavljanja ugaone brzine i obimskih napona, za potrebe projektovanja dobija se da je izotropni disk (čelik) od funkcionalnog materijala, sa parametrom nehomogenosti bolji izbor u odnosu na ortotropni disk (topaz ili barit) od funkcionalnog materijala, jer se kod izotropnog diska sa parametrom nehomogenosti javljaju manji obimski naponi u odnosu na ortotropni disk.

INTRODUCTION

Evaluation of the analytical and numerical solutions of rotating disks is always an important topic for research purposes as it has wide applications in fields of engineering design, aerospace industry, etc. Every material has some extent of elasticity. With the help of material elasticity, Sadd /1/ and Timoshenko et al. /2/ analysed the stress, displacement, strength and stiffness of the material. For the plastic state, these properties have been discussed by Chakrabarty, /3/. When composition or structure of the material changes which results in change of properties of that material then the material is said to be functionally graded. Suresh et al. /4/ have discussed the structure, properties and fundamentals of these functionally graded materials. You et al. /5/ applied numerical method to evaluate the stresses and deformations in an elastic-plastic rotating disk and said that their results and those obtained from finite element analysis have a good agreement. Heterogeneous materials are composites made up of different materials having different properties but same volume compositions. Negi et al. /6/ evaluated the transitional deformations in heterogeneous materials with results in the large triaxiality values for low strain hardening materials. Sharma et al. /7-8/ applied classical theory for obtaining the stresses and strains using finite difference method and concluded that functionally graded material is better alternative than homogeneous material as hoop stresses are less for functionally graded material than for the homogeneous material. Micro polar theory has been used by Yadav et al. /9/ to obtain numerical stresses in hollow thick-walled circular cylinder. The power-law distribution has been used by Bayat et al. /10/ to calculate the analytical and semi-analytical solutions for the hollow and solid disk by varying material properties and thickness profile. From the discussion, the author concludes that non-uniform thickness profile gives more efficient result than the uniform thickness profile for the functionally graded disk. Zheng et al. /11/ derived the constituent equation for the stress field and then evaluated the stresses for the disk with non-uniform thickness profile using finite difference method. They found that shear stress causes a change in location of principal stress. Dai et al. /12/ studied the effect of material properties for functionally graded magneto electro elastic disk and a semi-analytical method has been used to evaluate the numerical results. Generalized differ-

ential quadrature method has been used by Zharfi et al. /13/ to analyse the creep stresses in thin functionally graded disk. Effect of disk material and geometry over mechanical responses for the functionally graded disk whose thickness varies with power law distribution has been investigated by Bayat et al. /14/ with the help of shear deformation theory. Seba et al. /15/ analysed the elasticity and plasticity in reinforced composite materials by discretizing the reinforced material. They considered von-Mises two-dimensional model with positive linear hardening to analyse the plasticity of the material. Asghari et al. /16/ evaluated a two-dimensional solution for a rotating functionally graded solid and hollow disk, and found that the two-dimensional solution does not provide appropriate results in case of thick disks. Hence, they introduced a three-dimensional solution for thick disks which is a generalization of the two-dimensional solution. Bayat et al. /17/ considered different thickness profiles using power-law distribution for a rotating functionally graded disk under thermal field and found that non-uniform thickness profile gives smaller stresses and displacement which leads to better results. Dai et al. /18/ applied a semi-empirical method to evaluate the stresses and displacement components in a hollow circular functionally graded disk under temperature field, whose material properties vary with volume fraction of the material. Zafarmand et al. /19/ obtained a solution using nonlinear graded finite element method for uniform and non-uniform distributions of the functionally graded disk made up of single-walled carbon nanotubes.

All the above authors used classical theory to calculate the stress-strain and displacement fields in which they need to consider semi-empirical laws for the creation of the link between elastic and plastic states. While transition theory works in between fully elastic and fully plastic region, the fully elastic and fully plastic are the two extremes of the material. The state in between these two extreme points is known as transition state where the material shows some elasticity and some plasticity. Transition theory works in the transition region where no yield surface has been considered.

Borah /20/ applied Seth's transition theory in case of a shell to obtain the transitional and plastic stresses and strains. Sharma et al. /21-22/ evaluated the thermal transitional stresses for circular cylinder with internal and external pressure to minimize the possibility of fracture. Sharma et al. /23/ evaluated creep stresses for functionally graded disk and concluded that isotropic material is a better alternative than orthotropic material for engineering design. Sharma et al. /24/ and Aggarwal et al. /25/ have discussed the transitional stresses for pressurized circular cylinder and found that high functionally graded material is a better choice for engineering design. Sharma et al. /26/ discussed creep stresses for the functionally graded cylinder and found that higher the non-homogeneity and nonlinearity in material, better are the results. Safety analysis of a thick-walled circular cylinder with pressure at internal and external surface with thermal effects has been done by Sharma et al. /27-29/, and the same without the thermal effect has been done by Aggarwal et al. /30/ by using the concept of generalized principal strain measure. Sharma et al. /31/ discussed the effect of compressibility in a thick-walled cylinder with external pressure and found that highly compressible cylinders are a better substitute in designing purposes, irrespective of the material to be homogeneous or non-homogeneous. Creep stresses in a pressurized cylinder whose thickness and density varies, have been obtained by Sharma et al. /32/ and found that in the field of engineering design, the highly non-homogeneous material is a more preferable material. Sharma et al. /33/ applied the analytical method to obtain thermal stresses for a pressurized circular cylinder and deduced that the pressurized thermal cylinder with less compressibility is a better alternative.

In this paper, we have evaluated elastic-plastic stresses using transition theory in a thin rotating circular disk made up of orthotropic material whose thickness and density vary exponentially. The graphical results have been obtained for various non-homogeneous and nonlinear parameters.

BASIC CONSTITUENTS OF THE PROBLEM

Consider a functionally graded thin rotating disk with internal radius a and external radius b. The rotating disk with angular speed ω is considered to have variable thickness and variable density. In cylindrical polar co-ordinates, the displacements are given by

$$\theta = r(1-\beta), \quad \phi = 0 \quad \text{and} \quad \xi = \gamma z\,, \tag{1}$$

where: $\beta = \beta(r)$; and γ is a constant.

The generalized principal strain measure /20/ is

$$e_{ii} = \frac{1}{n}\left[1-(1-2e_{ii}^{A})^{n/2}\right], \quad (i=1,2,3)\,,$$

where: n is nonlinear measure; and e_{ii}^{A} be finite components of principal strain.

The strain components obtained by above generalized principal strain measure are

$$e_{rr} = \frac{1}{n}\left[1-(r\beta'+\beta)^{n}\right], \quad e_{\theta\theta} = \frac{1}{n}\left[1-\beta^{n}\right],$$

$$e_{zz} = \frac{1}{n}\left[1-(1-\gamma)^{n}\right], \quad e_{r\theta} = e_{\theta z} = e_{zr} = 0\,, \tag{2}$$

where: $\beta' = d\beta/dr$.

Stress components for orthotropic materials are given by

$$T_{rr} = A_{11}[1-(r\beta'+\beta)^{n}] + A_{12}[1-\beta^{n}] + A_{13}[1-(1-\gamma)^{n}]\,,$$

$$T_{\theta\theta} = A_{21}[1-(r\beta'+\beta)^{n}] + A_{22}[1-\beta^{n}] + A_{23}[1-(1-\gamma)^{n}]\,, \tag{3}$$

$$T_{zz} = 0\,.$$

Non-homogeneity in orthotropic material is considered as

$$A_{11} = \frac{A_{011}}{n}\left(\frac{r}{b}\right)^{K}, \; A_{12} = \frac{A_{012}}{n}\left(\frac{r}{b}\right)^{K}, \; A_{13} = \frac{A_{013}}{n}\left(\frac{r}{b}\right)^{K},$$

$$A_{21} = \frac{A_{021}}{n}\left(\frac{r}{b}\right)^{K}, \; A_{22} = \frac{A_{022}}{n}\left(\frac{r}{b}\right)^{K}, \; A_{23} = \frac{A_{023}}{n}\left(\frac{r}{b}\right)^{K},$$

where: $a \le r \le b$; A_{011}, A_{012}, A_{013}, A_{021}, A_{022}, A_{023}, A_{031}, A_{032}, A_{033} are material constants; and $K \ge 0$ is non-homogeneity parameter.

Using non-homogeneity of the materials in Eq.(3), we get

$$T_{rr}=\frac{A_{011}}{n}\left(\frac{r}{b}\right)^K[1-(r\beta'+\beta)^n]+\frac{A_{012}}{n}\left(\frac{r}{b}\right)^K[1-\beta^n]+\frac{A_{013}}{n}\left(\frac{r}{b}\right)^K[1-(1-\gamma)^n],$$

$$T_{\theta\theta}=\frac{A_{021}}{n}\left(\frac{r}{b}\right)^K[1-(r\beta'+\beta)^n]+\frac{A_{022}}{n}\left(\frac{r}{b}\right)^K[1-\beta^n]+\frac{A_{023}}{n}\left(\frac{r}{b}\right)^K[1-(1-\gamma)^n], \quad (4)$$

$$T_{zz}=0.$$

Equation of equilibrium is given by

$$\frac{d}{dr}(hrT_{rr})-hT_{\theta\theta}+h\rho\omega^2r^2=0, \quad (5)$$

where: thickness and density of rotating disk vary as $h = h_0 e^{-s(r/b)^{m_1}}$, $\rho=\rho_0 e^{t(r/b)^{m_2}}$, respectively with m_1, m_2 as thickness and density parameters.

OBJECTIVE OF THE PROBLEM

Substitution of Eq.(4) in Eq.(5) gives the following integro-differential equation,

$$\frac{e^{-s\left(\frac{r}{b}\right)^{m_1}}r^{K+1}}{b^K}\left[B_1-A_{011}(r\beta'+\beta)^n-A_{012}\beta^n\right]+n\rho_0\omega^2\int e^{-s\left(\frac{r}{b}\right)^{m_1}+t\left(\frac{r}{b}\right)^{m_2}}r^2dr-\int e^{-s\left(\frac{r}{b}\right)^{m_1}}\left(\frac{r}{b}\right)^K\left[B_2-A_{021}(r\beta'+\beta)^n-A_{022}\beta^n\right]dr=C_1 \quad (6)$$

where: $B_1 = [A_{011} + A_{012} + A_{013}(1 - (1 - \gamma)^n)]$, $B_2 = [A_{021} + A_{022} + A_{023}(1 - (1 - \gamma)^n)]$, and C_1 is an integration constant.

On further substitution of $r = 1/z$, and differentiating with respect to z, Eq.(6) becomes

$$D_1z^{-m_1}-\left[D_2z^{-m_1}+D_3\right](\beta-z\beta')^n-\left[D_4z^{-n}+D_5\right]\beta^n+D_6+z^2nA_{011}(\beta-z\beta')^{n-1}\beta''-znA_{012}\beta^{n-1}\beta'-D_7e^{-t(zb)^{-m_2}}z^{K-2}=0 \quad (7)$$

where: $D_1 = B_1sm_1b^{-m1}$, $D_2 = m_1sb^{-m1}A_{011}$, $D_3 = (-K - 1)A_{011} + A_{021}$, $D_4 = sm_1b^{-m1}A_{012}$, $D_5 = (-K - 1)A_{012} + A_{022}$, $D_6 = B_1(-K - 1) + B_2$, $D_7 = n\rho_0Q\omega^2b^K$.

Substitution of $z = e^l$ and $\beta = pe^{l/2}$ in Eq.(7) yields,

$$D_1e^{-\left(m_1+\left(\frac{n}{2}\right)\right)l}-\left(D_2e^{-m_1l}+D_3\right)\left(\frac{p}{2}-p'\right)^n-\left(D_4e^{-m_1l}+D_5\right)p^n-nA_{012}p^{n-1}\left(\frac{p}{2}+p'\right)+nA_{011}\left(\frac{p}{2}-p'\right)^{n-1}\left(p''-\frac{p}{4}\right)+$$

$$+D_6e^{-nl/2}-D_7e^{-t(e^{-lm_2})b^{-m_2}}e^{-\left(-K+2+\left(\frac{n}{2}\right)\right)l}=0, \quad (8)$$

where: $p' = dp/dt$.

On further substitution, $\frac{p}{2}+p'=q$ in Eq.(8), we get the following ordinary nonlinear differential equation,

$$\left[\left(2D_7e^{-t(e^{-l}b)^{-m_2}}e^{-\left(-K+2+\left(\frac{n}{2}\right)\right)l}-2D_6e^{-nl/2}-2D_1e^{-\left(m_1+\left(\frac{n}{2}\right)\right)l}\right)p^{-n}+2nA_{012}\frac{q}{p}+2\left(D_4e^{-m_1l}+D_5\right)+2\left(D_2e^{-m_1l}+D_3\right)\left(1-\frac{q}{p}\right)^n+\right.$$

$$\left.+nA_{011}\frac{q}{p}\left(1-\frac{q}{p}\right)^{n-1}\right]\frac{dp}{dq}=2nA_{011}\left(1-\frac{q}{p}\right)^{n-1}\left(\frac{q}{p}-\frac{1}{2}\right). \quad (9)$$

By substituting $q/p = F$, $1/p = Q$, Eq.(9) becomes

$$\frac{dQ}{dF}=\frac{2nA_{011}Q(1-F)^{n-1}\left(F-\frac{1}{2}\right)}{\left(-2\left(D_7e^{-t(e^{-l}b)^{-m_2}}e^{-(-K+2+(n/2))l}-D_6e^{-nl/2}-D_1e^{-(m_1+(n/2))l}\right)Q^n-2nA_{012}F-2\left(D_2e^{-m_1l}+D_3\right)(1-F)^n-\right.}$$
$$\left.-2\left(D_4e^{-m_1l}+D_5\right)-nA_{011}F(1-F)^{n-1}+2nFA_{011}(1-F)^{n-1}\left(F-\frac{1}{2}\right)\right)}. \quad (10)$$

The transition points in above equation are $F \to 1$ and $F \to \pm\infty$.

The boundary conditions are given as

$T_{rr} = 0$ at $r = a$, and (11a)

$T_{rr} = \sigma_0$ at $r = b$. (11b)

SOLUTION THROUGH PRINCIPAL STRESS

For obtaining the stresses and angular speed at the transition point $F \to \pm\infty$, the transition function R in terms of T_{rr} can be defined as

$$R = B^* - \frac{nT_{rr}}{\left(\frac{r}{b}\right)^K \left[A_{011}+A_{012}+A_{013}\right]} - \frac{n\rho\omega^2 r^2}{2\left(\frac{r}{b}\right)^K \left[A_{011}+A_{012}+A_{013}\right]} \quad (12)$$

The logarithmic differentiation with respect to r of Eq.(12) gives

$$R = C_2^* r^{G_2} e^{\frac{G_1 r^{m_1}}{m_1}}, \quad (13)$$

where: $G_1 = sm_1 b^{-m_1}$, $G_2 = [(-K-1)A_{011} + A_{021}]/A_{011}$ and C_2^* is the integration constant.

Comparison on Eq.(12) and Eq.(13) gives

$$T_{rr} = \left(\frac{r}{b}\right)^K \frac{B^* D}{n} - \frac{C_2^* D r^{G_2} e^{\frac{G_1 r^{m_1}}{m_1}}}{n}\left(\frac{r}{b}\right)^K - \frac{\rho_0 e^{t\left(\frac{r}{b}\right)^{m_2}} \omega^2 r^2}{2} \quad (14)$$

where: $D = A_{011} + A_{012} + A_{013}$.

Using Eq.(11a) in Eq.(14), we get

$$C_2^* = \frac{B^*}{a^{G_2} e^{G_1 a^{m_1}/m_1}} - \frac{n\rho_0\omega^2 e^{t(a/b)^{m_2}} a^{-K+2-G_2}}{2Db^{-K} e^{G_1(a^{m_1}/m_1)}}. \quad (15)$$

Using Eq.(11b) and Eq.(15) in Eq.(14), we get

$$\rho_0\omega^2 a^2 = \frac{\frac{2DB^*}{ne^t}\left(\frac{a}{b}\right)^2 \left\{1 - e^{s\left[1-\left(\frac{a}{b}\right)^{m_1}\right]}\left(\frac{a}{b}\right)^{-G_2}\right\} - \frac{2\sigma_0}{e^t}\left(\frac{a}{b}\right)^2}{1 - e^{t\left[\left(\frac{a}{b}\right)^{m_2}-1\right]} e^{s\left[1-\left(\frac{a}{b}\right)^{m_1}\right]}\left(\frac{a}{b}\right)^{-K+2-G_2}}. \quad (16)$$

Transitional stresses and angular speed at initial yielding are

$$T_{rr} = \frac{DB^*}{n}\left(\frac{r}{b}\right)^K \left[1 - \left(\frac{r}{a}\right)^{G_2} e^{s\left(\left(\frac{r}{b}\right)^{m_1} - \left(\frac{a}{b}\right)^{m_1}\right)}\right] - \frac{\rho_0\omega^2 a^2}{2}\left[e^{t\left(\frac{r}{b}\right)^{m_2}}\left(\frac{r}{a}\right)^2 - e^{s\left(\left(\frac{r}{b}\right)^{m_1} - \left(\frac{a}{b}\right)^{m_1}\right) + t\left(\frac{a}{b}\right)^{m_2}}\left(\frac{r}{a}\right)^{G_2+K}\right], \quad (17)$$

$$T_{\theta\theta} = \frac{DB^*}{n}\left(\frac{r}{b}\right)^K \left[(K+1) - (G_2+K+1)\left(\frac{r}{a}\right)^{G_2} e^{s\left(\left(\frac{r}{b}\right)^{m_1} - \left(\frac{a}{b}\right)^{m_1}\right)} - sm_1\left(\frac{r}{b}\right)^{m_1}\right] + \frac{\rho_0\omega^2 a^2}{2} \times$$

$$\times \left[e^{t\left(\frac{r}{b}\right)^{m_2}}\left(\frac{r}{a}\right)^2 \left(3 - m_2 t\left(\frac{r}{b}\right)^{m_2} + sm_1\left(\frac{r}{b}\right)^{m_1}\right) + e^{s\left(\left(\frac{r}{b}\right)^{m_1} - \left(\frac{a}{b}\right)^{m_1}\right) + t\left(\frac{a}{b}\right)^{m_2}}\left(\frac{r}{a}\right)^{G_2+K}(G_2+K+1)\right], \quad (18)$$

and

$$\omega^2 = \frac{\frac{2DB^*}{ne^t}\left\{1 - e^{s\left[1-\left(\frac{a}{b}\right)^{m_1}\right]}\left(\frac{a}{b}\right)^{-G_2}\right\} - \frac{2\sigma_0}{e^t}}{\rho_0 b^2 \left\{1 - e^{t\left[\left(\frac{a}{b}\right)^{m_2}-1\right]} e^{s\left[1-\left(\frac{a}{b}\right)^{m_1}\right]}\left(\frac{a}{b}\right)^{-K+2-G_2}\right\}}. \quad (19)$$

For fully plastic state, $A_{011} = A_{012} = A_{013}$, $A_{021} = A_{022} = A_{023}$.

Hence, the stresses and angular speed at fully plastic state are

$$T_{rr} = \frac{3A_{011}B^*}{n}\left(\frac{r}{b}\right)^K \left[1 - \left(\frac{r}{a}\right)^{G_2} e^{s\left(\left(\frac{r}{b}\right)^{m_1} - \left(\frac{a}{b}\right)^{m_1}\right)}\right] - \frac{\rho_0\omega^2 a^2}{2}\left[e^{t\left(\frac{r}{b}\right)^{m_2}}\left(\frac{r}{a}\right)^2 - e^{s\left(\left(\frac{r}{b}\right)^{n_1} - \left(\frac{a}{b}\right)^{n_1}\right) + t\left(\frac{a}{b}\right)^{m_2}}\left(\frac{r}{a}\right)^{G_2+K}\right], \quad (20)$$

$$T_{\theta\theta} = \frac{3A_{011}B^*}{n}\left(\frac{r}{b}\right)^K \left[(K+1) - (G_2+K+1)\left(\frac{r}{a}\right)^{G_2} e^{s\left(\left(\frac{r}{b}\right)^{m_1} - \left(\frac{a}{b}\right)^{m_1}\right)} - sm_1\left(\frac{r}{b}\right)^{m_1}\right] + \frac{\rho_0\omega^2 a^2}{2} \times$$

$$\times\left[e^{t\left(\frac{r}{b}\right)^{m_2}}\left(\frac{r}{a}\right)^2\left(3-m_2t\left(\frac{r}{b}\right)^{m_2}+sm_1\left(\frac{r}{b}\right)^{m_1}\right)+e^{s\left(\left(\frac{r}{b}\right)^{m_1}-\left(\frac{a}{b}\right)^{m_1}\right)+t\left(\frac{a}{b}\right)^{m_2}}\left(\frac{r}{a}\right)^{G_2+K}(G_2+K+1)\right], \tag{21}$$

and

$$\omega^2=\frac{\dfrac{6A_{011}B^*}{ne^t}\left\{1-e^{s\left[1-\left(\frac{a}{b}\right)^{m_1}\right]}\left(\frac{a}{b}\right)^{-G_2}\right\}-\dfrac{2\sigma_0}{e^t}}{\rho_0b^2\left\{1-e^{t\left[\left(\frac{a}{b}\right)^{m_2}-1\right]}e^{s\left[1-\left(\frac{a}{b}\right)^{m_1}\right]}\left(\frac{a}{b}\right)^{-K+2-G_2}\right\}}. \tag{22}$$

Now, we convert the above dimensional quantities in the following non-dimensional quantities as

$$R=\frac{r}{b},\ R_0=\frac{a}{b},\ \tau_{rr}=\frac{T_{rr}}{Y},\ \tau_{\theta\theta}=\frac{T_{\theta\theta}}{Y},\ \Omega_i^2=\frac{\rho_0\omega^2a^2}{Y_i},\ \Omega_f^2=\frac{\rho_0\omega^2b^2}{Y_f},\ B_i^*=\frac{B^*}{Y_i},\ B_f{}^*=\frac{B^*}{Y_f},$$

where: Y_i and Y_f are yield stress at initial and fully plastic state, respectively.

Transitional stresses and angular speed required for initial yielding from Eqs.(17-19) become

$$\tau_{rr}=\frac{DB_i^*}{n}R^K\left[1-\left(\frac{R}{R_0}\right)^{G_2}e^{s(R^{m_1}-R_0{}^{m_1})}\right]-\frac{\Omega_i^2}{2}\left[e^{tR^{m_2}}\left(\frac{R}{R_0}\right)^2-e^{s(R^{m_1}-R_0{}^{m_1})+tR_0^{m_2}}\left(\frac{R}{R_0}\right)^{G_2+K}\right], \tag{23}$$

$$\tau_{\theta\theta}=\frac{DB_i^*}{n}R^K\left[(K+1)-(G_2+K+1)\left(\frac{R}{R_0}\right)^{G_2}e^{s(R^{m_1}-R_0^{m_1})}-sm_1R^{m_1}\right]+\frac{\Omega_i^2}{2}\times$$

$$\times\left[e^{tR^{m_2}}\left(\frac{R}{R_0}\right)^2(3-m_2tR^{m_2}+sm_1R^{m_1})+e^{s(R^{m_1}-R_0^{m_1})+tR_0^{m_2}}\left(\frac{R}{R_0}\right)^{G_2+K}(G_2+K+1)\right], \tag{24}$$

and

$$\Omega_i^2=\frac{2DB_i^*R_0^2\left[1-e^{s(1-R_0^{m_1})}R_0^{-G_2}\right]-\dfrac{2n\sigma_0R_0^2}{Y_i}}{ne^t\left[1-e^{t(R_0^{m_2}-1)}e^{s(1-R_0^{m_1})}R_0^{-K+2-G_2}\right]}. \tag{25}$$

The stresses and angular speed at fully plastic state from Eqs.(20-22) become

$$\tau_{rr}=\frac{3A_{011}B_f{}^*}{n}R^K\left[1-\left(\frac{R}{R_0}\right)^{G_2}e^{s(R^{m_1}-R_0^{m_1})}\right]-\frac{\Omega_f^2R_0^2}{2}\left[e^{tR^{m_2}}\left(\frac{R}{R_0}\right)^2-e^{s(R^{m_1}-R_0^{m_1})+tR_0^{m_2}}\left(\frac{R}{R_0}\right)^{G_2+K}\right], \tag{26}$$

$$\tau_{\theta\theta}=\frac{3A_{011}B_f{}^*}{n}R^K\left[(K+1)-(G_2+K+1)\left(\frac{R}{R_0}\right)^{G_2}e^{s(R^{m_1}-R_0^{m_1})}-sm_1R^{m_1}\right]+\frac{\Omega_f^2R_0^2}{2}\times$$

$$\times\left[e^{tR^{m_2}}\left(\frac{R}{R_0}\right)^2(3-m_2tR^{m_2}+sm_1R^{m_1})+e^{s(R^{m_1}-R_0^{m_1})+tR_0^{m_2}}\left(\frac{R}{R_0}\right)^{G_2+K}(G_2+K+1)\right], \tag{27}$$

and

$$\Omega_f^2=\frac{6A_{011}B_f{}^*\left[1-e^{s(1-R_0^{m_1})}R_0^{-G_2}\right]-\dfrac{2n\sigma_0}{Y_f}}{ne^t\left[1-e^{t(R_0^{m_2}-1)}e^{s(1-R_0^{m_1})}R_0^{-K+2-G_2}\right]}. \tag{28}$$

NUMERICAL OUTCOMES AND DISCUSSION

The numerical and graphical results of angular speed and circumferential stresses required for initial yielding and full plasticity have been obtained by substituting the following combinations of thickness and density parameters: s_1 = 0.1, 0.4; m_1 = 0.2, 0.3; t = 0.2, 0.3; and m_2 = 0.1, 0.4; σ_0 = 0.5. and B^* = 5 in Eqs.(24), (25), (27) and (28). The relation between non-homogeneity parameter and angular speed required for initial yielding and full plasticity by varying the radii ratio can be seen in Figs. 1-4, while Figs. 5-8 show the graphical relation between circumferential stresses (for initial yielding and full plasticity) and radii ratio for various thickness and density parameters. The above discussion has been done for three different materials whose material properties are as follows.

Table 1: Values of material constants for different materials (in units of 10^{11} N/m^2)

Material	A_{011}	A_{012}	A_{013}	A_{021}	A_{022}	A_{023}
barite (orthotropic)	0.8941	0.4614	0.2691	0.4614	0.7842	0.2676
steel (isotropic)	5.326	3.688	3.688	3.688	5.326	3.688
topaz (orthotropic)	2.8145	1.2552	0.8433	1.2552	3.4911	0.8825

The following numerical values and graphical results have been evaluated using data from Table 1.

Table 2 shows angular speeds and percentage increase in angular speed required from initial yielding to full plasticity for the various functionally graded disk with thickness, density and nonlinearity parameters as: s = 0.1; m_1 = 0.2; t = 0.3; m_2 = 0.4; and n = 1/3 for different radii ratios and non-homogeneity parameters. From Table 2, it can also be analysed that as non-homogeneity of the disk increases, the angular speed increases, but percentage increase in angular speed required from initial yielding to full plasticity decreases.

Table 2. Angular speed against radii ratios for functionally graded disk having exponentially variable thickness and density.

n = 1/3; s = 0.1; m_1 = 0.2; t = 0.3; and m_2 = 0.4			Angular speed			Percentage increase in angular speed required from initial yielding to full plasticity		
			R_0 = 0.3	R_0 = 0.5	R_0 = 0.7	R_0 = 0.3	R_0 = 0.5	R_0 = 0.7
K = 1	barite	Ω_i^2	7.60407	22.417	39.9273	173.898	49.55854	4.686884
		Ω_f^2	57.0458	50.1418	43.7577			
	topaz	Ω_i^2	9.33433	24.2068	42.3402	150.0849	46.1452	3.750278
		Ω_f^2	58.3792	51.7019	45.5755			
	steel	Ω_i^2	5.54399	13.7129	23.6738	216.5975	88.00761	33.92736
		Ω_f^2	55.5696	48.4708	42.4626			
K = 3	barite	Ω_i^2	9.575	33.3732	73.0123	166.3514	46.79914	2.90112
		Ω_f^2	67.928	71.9192	77.3101			
	topaz	Ω_i^2	11.0757	34.1826	72.9775	148.4042	45.38352	3.232799
		Ω_f^2	68.3422	72.2496	77.7722			
	steel	Ω_i^2	6.95041	20.9673	44.6796	215.4924	87.54227	33.64595
		Ω_f^2	69.1812	73.7464	79.8033			
K = 5	barite	Ω_i^2	9.75238	36.1122	89.224	165.8139	46.36639	2.505322
		Ω_f^2	68.9074	77.3636	93.7507			
	topaz	Ω_i^2	11.2324	36.6765	87.9899	148.2783	45.25753	3.110344
		Ω_f^2	69.2389	77.3865	93.5486			
	steel	Ω_i^2	7.07699	22.7809	54.9724	215.4144	87.47214	33.58651
		Ω_f^2	70.4063	80.0653	98.1002			

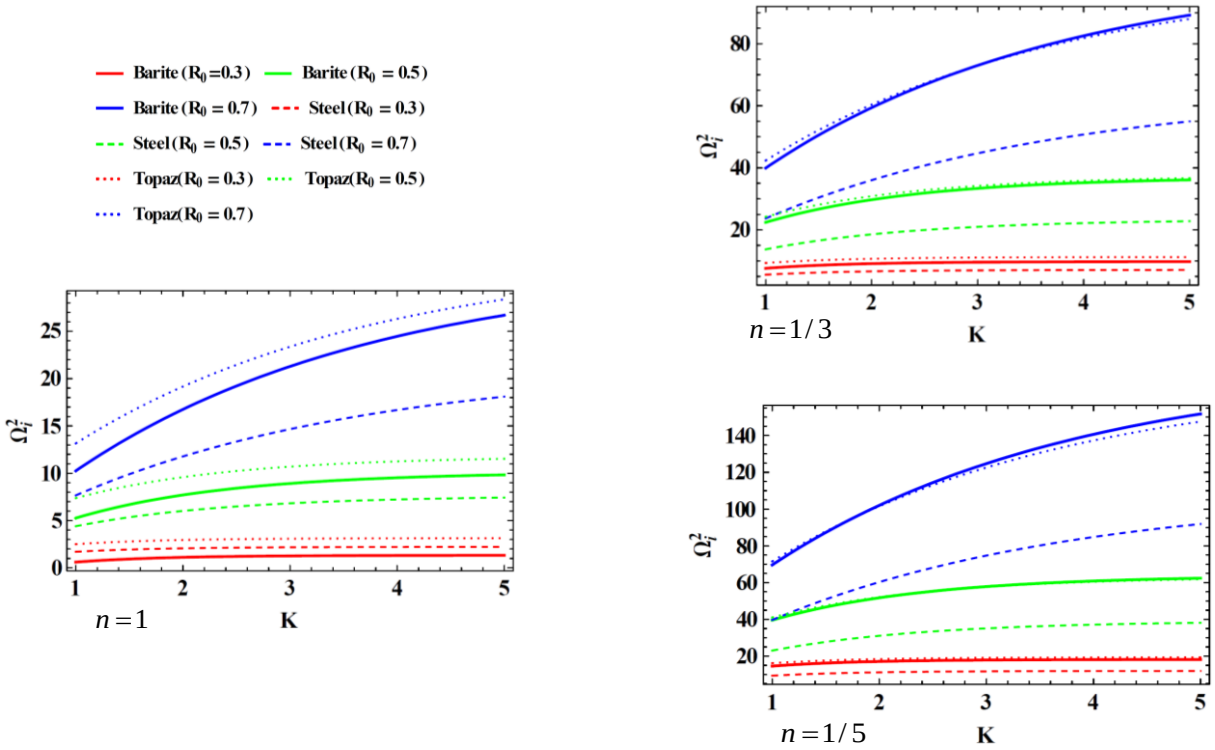

Figure 1. Angular speed required for initial yielding in a functionally graded rotating disk with: s = 0.1; m_1 = 0.2; t = 0.3; and m_2 = 0.4.

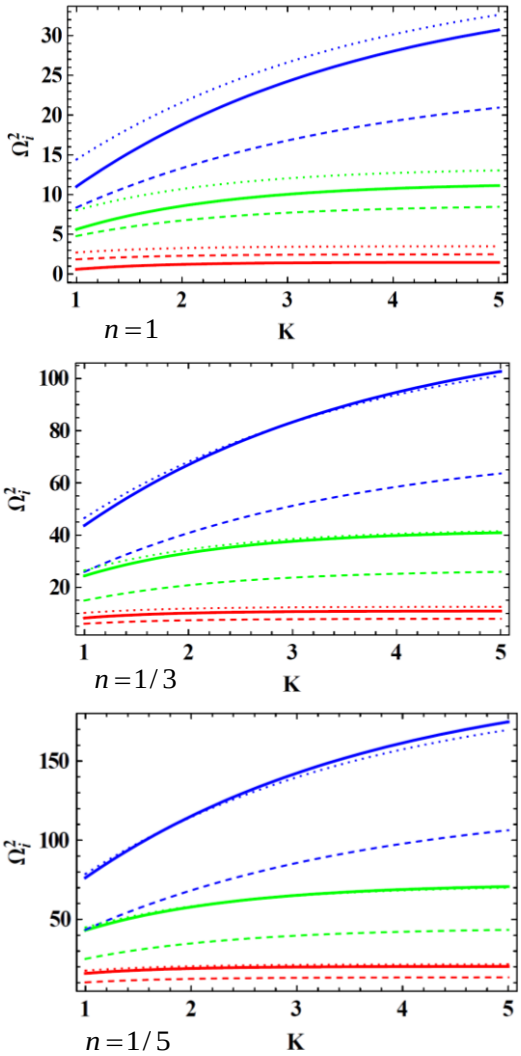

Figure 2. Angular speed required for initial yielding in a functionally graded rotating disk with: s = 0.4; m_1 = 0.3; t = 0.2; and m_2 = 0.1.

Figures 1-2 show the angular speed required for initial yielding in a functionally graded disk with variable thickness and density. It can be seen that the angular speed required for initial yielding in a functionally graded topaz is higher than functionally graded barite and steel. Also, it increases with increase in radii ratio and non-homogeneity parameter. Change in measure from linear to nonlinear and increase in nonlinearity gives an increase in angular speed for initial yielding. As the thickness and density decrease, the angular speed required for initial yielding increases which can be observed from Fig. 2.

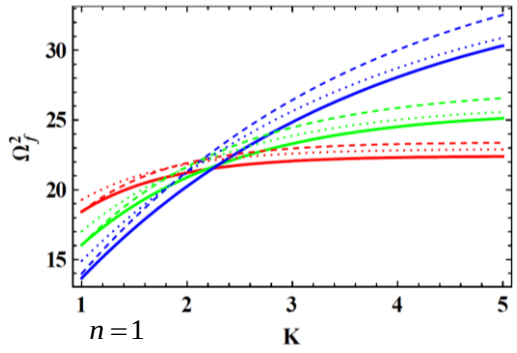

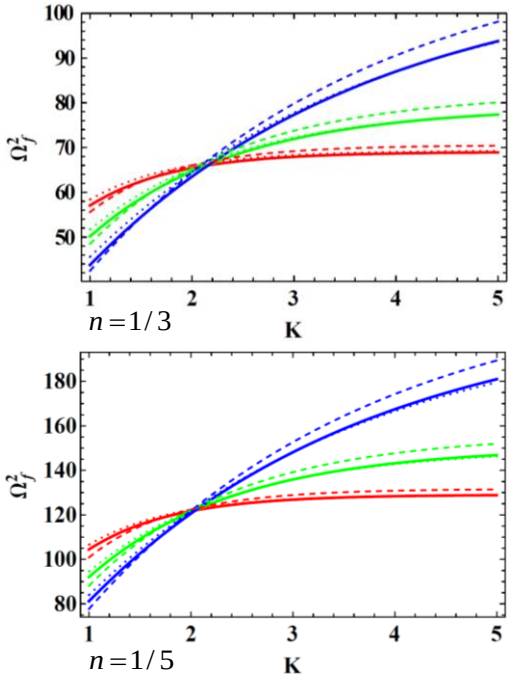

Figure 3. Angular speed required for full plasticity in a functionally graded rotating disk with: s = 0.1; m_1 = 0.2; t = 0.3; and m_2 = 0.4.

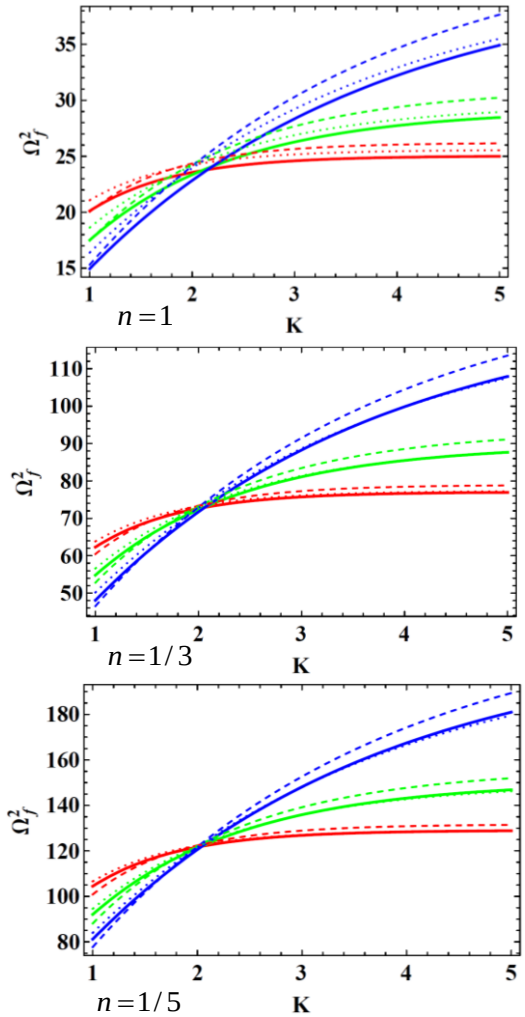

Figure 4. Angular speed required for full plasticity in a functionally graded rotating disk with: s = 0.4; m_1 = 0.3; t = 0.2; and m_2 = 0.1.

Graphical results of angular speed required for full plasticity verses non-homogeneity parameter are evaluated in Figs. 3-4. The effect of radii ratio and non-homogeneity parameters is significant on angular speed required for fully plastic state i.e. angular speed is maximum for K =1, R_0 = 0.3; K = 5, R_0 = 0.7. It can also be seen that angular speed required for full plasticity in functionally graded steel is on the higher side than the functionally graded barite and topaz. From Figs. 3 and 4, it can be noticed that angular speed required for full plasticity increases with decrease of thickness and density of the functionally graded disk.

Table 3 shows the circumferential stresses in the functionally graded disk whose thickness and density parameters are fixed as s = 0.1; m_1 = 0.2; t = 0.3; and m_2 = 0.4 for different radii ratios, nonlinearity, and non-homogeneity parameters. As the disk changes from linear to nonlinear, a drastic increase in stresses can be seen. Also, the stresses increase on increasing radii ratio and non-homogeneity parameter.

Table 3. Transitional stresses against radii ratios for functionally graded disk having exponentially variable thickness and density.

s = 0.1; m_1 = 0.2; t = 0.3; and m_2 = 0.4		n =1			n = 1/3		
		R = 0.55	R = 0.75	R = 0.95	R = 0.55	R = 0.75	R = 0.95
K = 1	barite	38.8842	62.3516	89.2798	133.533	217.168	315.963
		22.8815	37.333	54.5116	69.9145	114.265	167.156
	topaz	44.0571	71.2659	103.464	137.415	223.226	325.515
		23.8405	38.7721	56.6051	71.9141	117.022	170.948
	steel	24.705	40.8444	59.9971	75.4358	124.848	183.657
		21.9801	36.3852	53.5395	66.169	109.557	161.253
K = 3	barite	40.8727	89.6453	166.383	139.498	299.049	547.272
		23.8695	50.8958	92.8257	72.8788	154.953	282.098
	topaz	44.558	95.8071	175.552	138.922	296.858	541.794
		24.0992	51.4108	93.7286	72.6904	154.939	282.319
	steel	28.1279	59.4411	107.951	85.7047	180.639	327.519
		24.9616	52.5838	95.3093	75.1136	158.152	286.563
K = 5	barite	33.6861	87.153	210.773	117.939	291.572	680.444
		20.2984	49.6574	114.884	62.1653	151.238	348.274
	topaz	37.2705	92.9565	217.816	117.055	288.297	668.571
		20.3457	49.9413	115.49	61.4298	150.53	347.602
	steel	24.6002	58.7758	134.267	75.1215	178.643	406.467
		21.8888	52.0043	118.232	65.8952	156.414	355.33

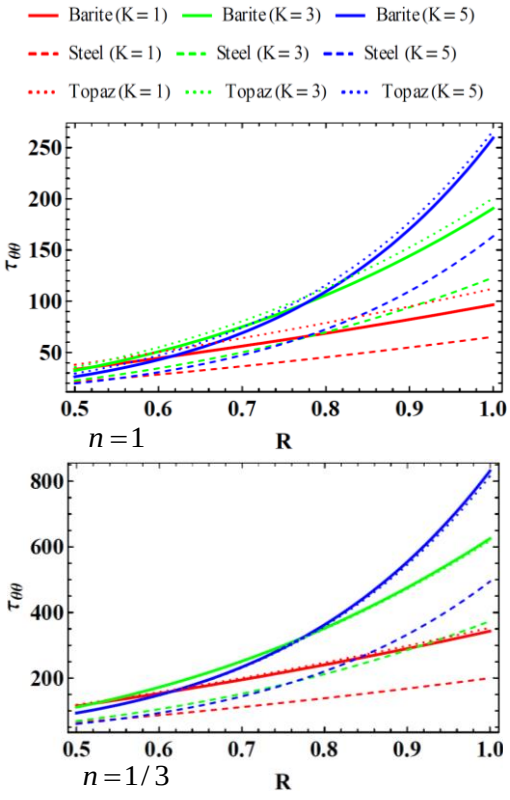

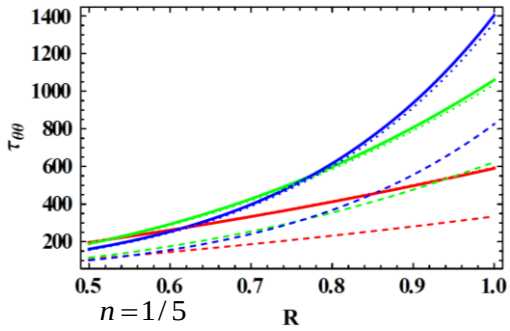

Figure 5. Transitional circumferential stress for functionally graded rotating disk with: s = 0.1; m_1 = 0.2; t = 0.3; and m_2 = 0.4.

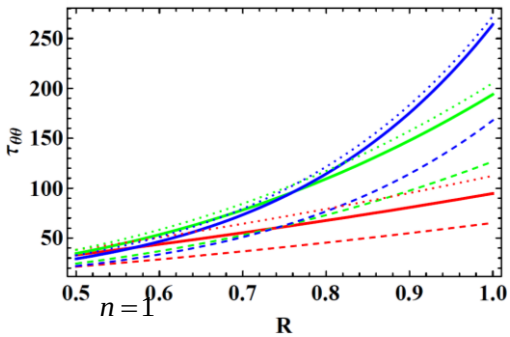

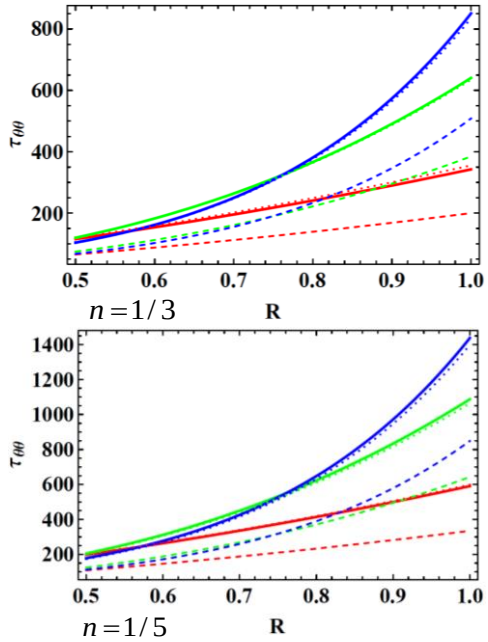

Figure 6. Transitional circumferential stresses for functionally graded rotating disk with: s = 0.4; m_1 = 0.3; t = 0.2; and m_2 = 0.1.

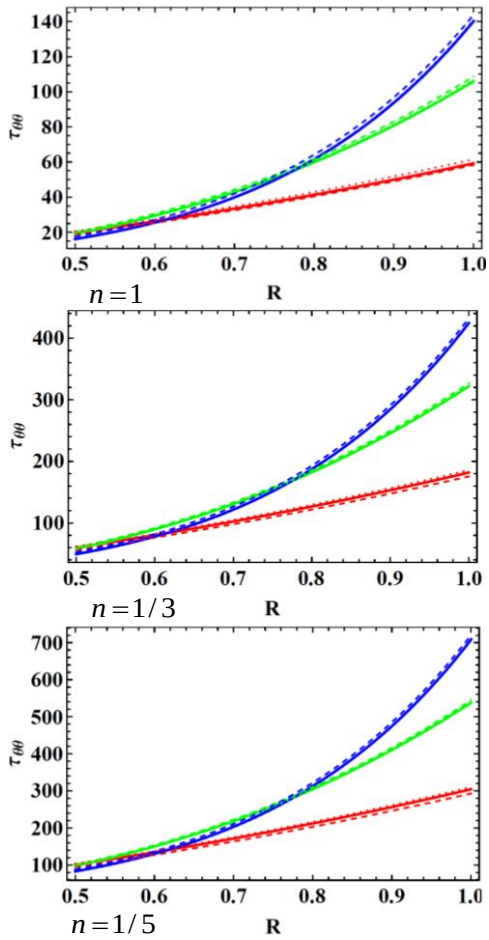

Figure 7. Fully plastic circumferential stress for functionally graded rotating disk with: s = 0.1; m_1 = 0.2; t = 0.3; and m_2 = 0.4.

It can be noticed from Figs. 5-6 that transitional circumferential stresses are higher at external surface with K = 5. As the non-homogeneity and radii ratio increases, the required transitional stresses decrease. In case of disk with linear measure, functionally graded topaz gives maximum transitional stresses while in case of nonlinear measure, maximum transitional stresses are obtained in disk made up of functionally graded barite. Increase in thickness parameter and decrease in density parameter gives rise in transitional circumferential stresses for functionally graded disk as can be observed from Fig. 6.

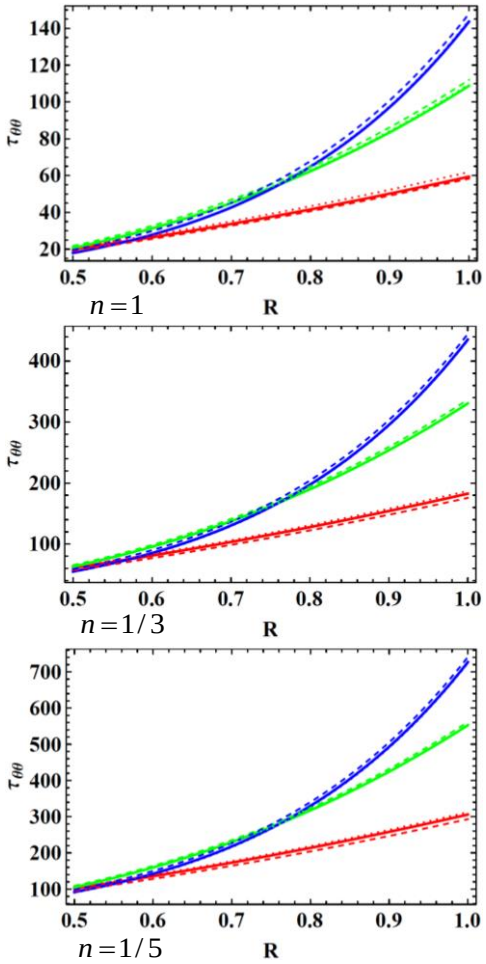

Figure 8: Fully plastic circumferential stress for functionally graded rotating disk with: s = 0.4; m_1 = 0.3; t = 0.2; and m_2 = 0.1.

From Figs. 7-8, we have analysed that fully plastic circumferential stresses increase on decreasing the thickness and density of the disk. It can be seen from figures that at external surface of the disk, functionally graded steel with K = 5 give higher circumferential stresses, while that with K = 1 give lower circumferential stresses. As the nonlinearity of the disk increases, the transitional stress for full plasticity also increases.

CONCLUSION

It has been analysed from the above numerical discussion of angular speed that functionally graded steel shows the higher percentage increase in angular speed required from initial yielding to full plasticity than functionally graded barite and functionally graded topaz. Also, as analysed from the graphical discussion of circumferential stresses that circumferential stresses obtained for functionally graded

steel with non-homogeneity parameter $K = 1$ are less than for functionally graded barite and topaz. Hence, it can be concluded that functionally graded steel with non-homogeneity parameter $K = 1$ is the best appropriate material for engineering design. Also, functionally graded barite with non-homogeneity parameter $K = 1$ is better choice than that of functionally graded topaz.

REFERENCES

1. Sadd, M.H., Elasticity: Theory, Applications and Numerics, Academic Press, Elsevier, 2005.
2. Timoshenko, S.P., Goodier, J.N., Theory of Elasticity, 3rd Ed., McGraw-Hill, New York, 1970.
3. Chakrabarty, J., Theory of Plasticity, 3rd Ed., Elsevier Butterworth-Heinemann, San Diego, 2006.
4. Suresh, S., Mortensen, A., Fundamentals of Functionally Graded Materials: Processing and Thermomechanical Behavior of Graded Metals and Metal-Ceramic Composites, London: IOM Comm. Ltd., 1998.
5. You, L.H., Tang, Y.Y., Zhang, J.J., Zheng, C.Y. (2000), *Numerical analysis of elastic-plastic rotating disks with arbitrary variable thickness and density*, Int. J Solids Struct. 37(52): 7809-7820. doi: 10.1016/S0020-7683(99)00308-X
6. Negi, V., Picu, R.C. (2018), *Elastic-plastic transition in stochastic heterogeneous materials: Size effect and triaxiality*, Mech. Mater. 120: 26-33. doi: 10.1016/j.mechmat.2018.02.004
7. Sharma, S., Yadav, S. (2019), *Numerical solution of thermal elastic-plastic functionally graded thin rotating disk with exponentially variable thickness and exponentially variable density*, Therm. Sci. 23(1): 125-136. doi: 10.2298/TSCI131001136S
8. Sharma, S., Yadav, S. (2013), *Thermo elastic-plastic analysis of rotating functionally graded stainless steel composite cylinder under internal and external pressure using finite difference method*, Advan. Mater. Sci. Eng. 2013: 11p. doi: 10.1155/2013/810508
9. Yadav, S., Sharma, S. (2018), *Torsion in microstructure hollow thick-walled circular cylinder made up of orthotropic material*, J Solid Mech. 10(3): 581-590.
10. Bayat, M., Saleem, M., Sahari, B.B., et al. (2008), *Analysis of functionally graded rotating disks with variable thickness*, Mech. Res. Comm. 35(5): 283-309. doi: 10.1016/j.mechrescom.2008.02.007
11. Zheng, Y., Bahaloo, H., Mousanezhad, D., et al. (2016), *Stress analysis in functionally graded rotating disks with non-uniform thickness and variable angular velocity*, Int. J Mech. Sci. 119: 283-293. doi: 10.1016/j.ijmecsci.2016.10.018
12. Dai, T., Dai, H.L. (2017), *Analysis of rotating FGMEE circular disk with variable thickness under thermal environment*, Appl. Math. Modelling, 45(C): 900-924. doi: 10.1016/j.apm.2017.01.007
13. Zharfi, H., Toussi, H.E. (2017), *Numerical creep analysis of FGM rotating disc with GDQ method*, J Theor. Appl. Mech. 55(1): 331-341. doi: 10.15632/jtam-pl.55.1.331
14. Bayat, M., Sahari, B.B., Salem, M., et al. (2009), *Thermo-elastic solution of a functionally graded variable thickness rotating disk with bending based on the first-order shear deformation theory*, Thin-Wall. Struct. 47(5): 568-582. doi: 10.1016/j.tws.2008.10.002
15. Seba, M.R., Kebdani, S., Sahli, A., Sahli, S. (2017), *Elastic-plastic analysis of reinforced composite materials*, J Mater. Eng. Struct. 4: 211-224.
16. Ashgari, M., Ghafoori, E. (2010), *A three-dimensional elasticity solution for functionally graded rotating disks*, Comp. Struct. 92(5): 1092-1099. doi: 10.1016/j.compstruct.2009.09.055
17. Bayat, M., Saleem, M., Sahari, B.B., et al. (2009), *Mechanical and thermal stresses in a functionally graded rotating disk with variable thickness due to radially symmetry loads*, Int. J Pres. Ves. Piping, 86(6): 357-372. doi: 10.1016/j.ijpvp.2008.12.006
18. Dai, T., Dai, H.L. (2016), *Thermo-elastic analysis of functionally graded rotating hollow circular disk with variable thickness and angular speed*, Appl. Math. Model. 40(17-18): 7689-7707. doi: 10.1016/j.apm.2016.03.025
19. Zafarmand, H., Kadkhodayan, M. (2015), *Nonlinear analysis of functionally graded nanocomposite rotating disks with variable thickness reinforced with carbon nanotubes*, Aerosp. Sci. Tech. 41: 47-54. doi: 10.1016/j.ast.2014.12.002
20. Borah, B.N. (2005), *Thermo-elastic-plastic transition*, Contemp. Math. 379: 93-111. doi: 10.1090/conm/379/07027
21. Sharma, S., Sahai, I., Kumar, R. (2014), *Thermo elastic-plastic transition of transversely isotropic thick-walled circular cylinder under internal and external pressure*, Multidisc. Model. Mater. Struct. 10(2): 211-227. doi: 10.1108/MMMS-03-2013-0026
22. Sharma, S. (2017), *Stress analysis of elastic-plastic thick-walled cylindrical pressure vessels subjected to temperature*, Struct. Integ. and Life, 17(2): 105-112.
23. Maheshwari, K., Sharma, S. (2020), *Creep stresses in functionally graded thin rotating orthotropic disk with variable thickness and density*, AIP Conf. Proc. 2214(1): 020011. doi: 10.1063/5.0003370
24. Sharma, S., Panchal, R. (2018), *Elastic-plastic transition of pressurized functionally graded orthotropic cylinder using Seth's transition theory*, J Solid Mech. 10(2): 450-463.
25. Aggarwal, A.K., Sharma, R., Sharma, S. (2013), *Safety analysis using Lebesgue strain measure of thick-walled cylinder for functionally graded material under internal and external pressure*, Scient. World J, 2013: 676190. doi: 10.1155/2013/676190
26. Sharma, S. (2017), *Creep transition in bending of functionally graded transversely isotropic rectangular plates*, Struct. Integ. and Life, 17(3): 187-192.
27. Sharma, S., Aggarwal, A.K., Sharma, R. (2013), *Safety analysis of thermal creep non-homogeneous thick-walled circular cylinder under internal and external pressure using Lebesgue strain measure*, Multidisc. Model. Mater. Struct. 9(4): 499-513.
28. Sharma, S., Yadav, S., Sharma, R. (2017), *Thermal creep analysis of functionally graded thick-walled cylinder subjected to torsion and internal and external pressure*, J Solid Mech. 9(2): 302-318.
29. Aggarwal, A.K., Sharma, R., Sharma, S. (2014), *Collapse pressure analysis of transversely isotropic thick-walled cylinder using Lebesgue strain measure and transition theory*, Scient. World J, 2014: 10p. doi: 10.1155/2014/240954
30. Sharma, S., Yadav, S., Radaković, Z. (2018), *Finite creep deformation in thick-walled circular cylinder with varying compressibility under external pressure*, Struct. Integ. and Life, 18(1): 31-36.
31. Sharma, S., Yadav, S., Sharma, R. (2018), *Creep torsion in thick-walled circular cylinder under internal and external pressure*, Struct. Integr. and Life, 18(2): 89-97.
32. Sharma, S., Panchal, R. (2018), *Creep stresses in functionally graded rotating orthotropic cylinder with varying thickness and density under internal and external pressure*, Struct. Integ. and Life, 18(2): 111-119.
33. Sharma, R., Sharma, S., Radaković Z. (2018), *Thermal creep analysis of pressurized thick-walled cylindrical vessels*, Struct. Integ. and Life, 18(1): 7-14.